Drying Simulation of Nanoparticle Suspension Film on Substrate

M Fujita* *and* ***Y Yamaguchi****
**The University of Tokyo, Tokyo, Japan*

Drying simulations of nanoparticle suspension films on a substrate are carried out by a three-dimensional simulator developed. The motion of nanoparticles in the suspension films is modeled by Langevin equation, in which forces exerted on each nanoparticle consist of contact force, capillary force, Brownian force, van der Waals force, electrostatic force and fluid drag force. The drying of suspension films is described as a variation of interface between gas and liquid with time. The present simulator is applied to drying processes of suspension films on a flat substrate, so that self-organized monolayer or multilayer structures of nanoparticles are formed after drying up depending on concentration of the suspension films. The structure formations are visualized with time, and planar structures of nanoparticles are evaluated temporally and quantitatively. The results indicate mechanisms of monolayer and multilayer structure formations of nanoparticles in the suspension films during drying.

1 Introduction

A focus in materials nanotechnology is to develop macro-scale materials that have some new mechanical, electrical or optical features by use of structure formation of nanoparticles with noticeable surface and quantum effects. Among the processes of structure formation of nanoparticles, coating-drying process using nanoparticle suspensions is expected to be one of the most promising approaches to practical fabrication of nanoparticle structures. In the process, a nanoparticle suspension is coated on a solid substrate followed by drying of the solvent, as shown in Figure 1. An autonomous structure formation of nanoparticles occurs during drying, and monolayer of nanoparticles[1-3] or multilayer of nanoparticles[4] is fabricated. The autonomous structure formation is called "self-organization" since it is a nonequilibrium process when the suspension flows or dries. It is important to clarify mechanism of the structure formation in order to control structure of nanoparticles by process parameters, namely, properties of nanoparticle, solvent, geometry and drying condition. However, it is difficult to investigate the mechanism theoretically because the structure formation of nanoparticles in a suspension is a multiple degree of freedom system in which various nonlinear forces are exerted on nanoparticles. In addition, it is difficult to obtain dynamics of the structure formation by existing experimental methods. On the other hand, numerical simulation is expected to be a

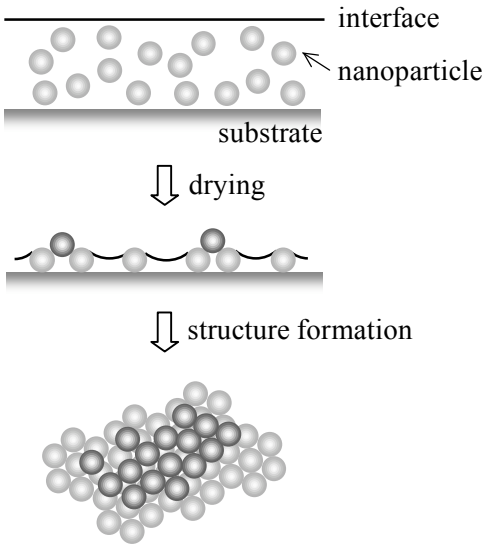

Fig. 1 A coating-drying process of nanoparticle suspensions on a substrate

more effective methodology in which the motion of nanoparticles are visualized with time and the structure of nanoparticles can be quantitatively evaluated. Our objective is to develop a three-dimensional structure formation simulator of nanoparticle suspensions during drying that is able to investigate the mechanism of structure formation and to clarify the relationship between process parameters and structures.

The nanoparticles in a suspension in a drying process are subject to multiscale forces by other nanoparticles, the substrate and the solvent. Lateral capillary immersion force[5] is exerted between nanoparticles on an interface. In addition, there are Brownian force, fluid drag force, contact force between nanoparticles or between nanoparticles and a substrate, electrostatic force and van der Waals force. Generally, Brownian force, electrostatic force and van der Waals force are ignored if the particles are sufficiently large, so that the motion of particles can be analyzed by continuous fluid dynamics and solid mechanics. If the particles are of molecular dimensions, the motion can be estimated by molecular dynamics. On the other hand, it is expected that a multidisciplinary and multiscale model is necessary to deal with nanoparticles in a suspension whose diameters are in the range from several nanometers to several hundred nanometers. Maenosono et al.[6] developed a two-dimensional numerical model to deal with the structure formation of nanoparticles in a suspension during drying, in which lateral capillary immersion force, contact force and fluid drag force are included. They obtained numerical results where the monolayer structure of nanoparticles is in good qualitative agreement with the scanning electron microscope images. Nishikawa et al.[7] developed an improved model that included an adequate screening effect of the capillary force by the neighboring nanoparticles and a periodic boundary condition. They obtained numerical results that represent the effect of the coverage ratio on the monolayer structure of nanoparticles. The authors also developed a two-dimensional model[8] in which Brownian force, electrostatic force, van der Waals force and friction force between nanoparticles and a solid substrate are newly introduced in order to accurately investigate the two-dimensional structure formation of nanoparticles.

All the models above mentioned are two-dimensional models that deal with planar motion of nanoparticles on a substrate. The models suppose that all the nanoparticles are deposited on the substrate before drying up for a dilute suspension. However, it is likely that some nanoparticles put on other nanoparticles before drying up for a dense suspension. Naturally, the two-dimensional models cannot deal with multilayer structure formation of nanoparticles. The authors used a preliminary three-dimensional model[9] that contains vertical motion of nanoparticles to deal with monolayer structure formation of nanoparticles in a dense suspension. In the present study, the authors develop a three-dimensional model that is able to deal with multilayer structure formation of nanoparticles in a suspension in industrial coating-drying processes.

2 Modeling

2.1 Equations of motion

Each nanoparticle is assumed to be a rigid sphere with the same diameter. The translational motion of *i*-th sphere is expressed by Langevin equation

$$m\frac{\partial \boldsymbol{V}_i}{\partial t} = \boldsymbol{F}_i \ , \tag{1a}$$

where

$$\boldsymbol{F}_i = \boldsymbol{F}_i^{\mathrm{co}} + \boldsymbol{F}_i^{\mathrm{ca}} + \boldsymbol{F}_i^{\mathrm{e}} + \boldsymbol{F}_i^{\mathrm{w}} - \xi \boldsymbol{V}_i + \boldsymbol{R} \ , \tag{1b}$$

The rotational motion of *i*-th sphere obeys the law of angular momentum conservation

$$I\frac{\partial \boldsymbol{\omega}_i}{\partial t} = \boldsymbol{T}_i^{\mathrm{co}} \ . \tag{2}$$

Figure 2 shows contact force and contact torque when two spheres contact with each other. They are modeled according to discrete element method (DEM)[10,11] as

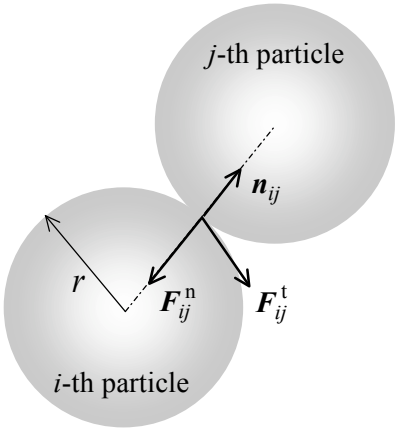

Fig. 2 Contact of two spheres

$$\boldsymbol{F}_i^{\mathrm{co}} = \sum_j \left(\boldsymbol{F}_{ij}^{\mathrm{n}} + \boldsymbol{F}_{ij}^{\mathrm{t}} \right) \tag{3}$$

$$\boldsymbol{T}_i^{\mathrm{co}} = \sum_j \left(r\boldsymbol{n}_{ij} \times \boldsymbol{F}_{ij}^{\mathrm{t}} \right) , \tag{4}$$

where j is an index of sphere or wall that contacts with i-th sphere. According to Voigt model and Hertzian contact theory, normal and tangential vector of the contact are expressed as a combination of elastic and damping forces, respectively, which are described in detail in Ref. (12).

Capillary force is given as a combination of lateral capillary immersion force and vertical capillary force as

$$\boldsymbol{F}_i^{\mathrm{ca}} = \sum_j f_{ij}^{\mathrm{l}} \boldsymbol{n}_{ij} + f_i^{\mathrm{v}} \boldsymbol{s}_i , \tag{5}$$

where j is an index of sphere or wall to which i-th sphere is connected by a meniscus. The lateral capillary immersion force is exerted when spheres on a substrate or other spheres protrude an interface. The magnitude of the force exerted between two spheres is approximately given[5] by

$$f_{ij}^{\mathrm{l}} = 2\pi\gamma Q^2 \big/ L_{ij} , \tag{6a}$$

where

$$Q = r_{\mathrm{c}} \sin\psi . \tag{6b}$$

The slope angle of interface on a sphere depends on contact angle and the height of interface. On the other hand, the vertical capillary force is exerted on all spheres that protrude the interface, and the magnitude is given by

$$f_i^{\mathrm{v}} = 2\pi\gamma Q . \tag{7}$$

The electrostatic force exerted between i-th sphere and j-th sphere is treated together with the van der Waals force in DLVO theory[13] as

$$\boldsymbol{F}_i^{\mathrm{e}} + \boldsymbol{F}_i^{\mathrm{w}} = \sum_j \left(f_{ij}^{\mathrm{e}} + f_{ij}^{\mathrm{w}} \right) \boldsymbol{n}_{ij} . \tag{8}$$

The magnitude of electrostatic repulsive force exerted on two homogeneously charged spheres is derived through Derjaguin's approximation[13] as

$$f_{ij}^{\mathrm{e}} = -\frac{64\pi r n k_{\mathrm{b}} T \Theta^2 e^{-\kappa H_{ij}}}{\kappa} \ , \tag{9a}$$

where

$$\Theta = \tanh\left(\frac{Ze\varphi}{4k_{\mathrm{b}}T}\right), \quad \kappa = \sqrt{\frac{2nZ^2e^2}{\varepsilon_0\varepsilon_{\mathrm{r}}k_{\mathrm{b}}T}} \ . \tag{9b}$$

The magnitude of van der Waals force is derived through a volume integration of the force exerted between two atoms that are contained in the bodies. In the case of two spheres,

$$f_{ij}^{\mathrm{w}} = \frac{Ar}{12H_{ij}^2} \ . \tag{10}$$

The magnitude of the Brownian force is given by the normal distribution random number[14]. The standard deviation is derived by using Eq. (1) and the law of three-dimensional energy equipartition as

$$\sigma = \sqrt{6\xi k_{\mathrm{b}} T / \Delta t} \ . \tag{11}$$

2.2 Solution algorithm

The non-dimensionalized Eqs. (1) and (2) are temporally integrated by Euler explicit method. The position and the rotation angle of each sphere at the next time step is obtained as

$$\boldsymbol{V}_i^{n+1} = \boldsymbol{V}_i^n + \Delta t \frac{\boldsymbol{F}_i^n}{m}, \quad \boldsymbol{X}_i^{n+1} = \boldsymbol{X}_i^n + \Delta t \boldsymbol{V}_i^n \ , \tag{12}$$

$$\boldsymbol{\omega}_i^{n+1} = \boldsymbol{\omega}_i^n + \Delta t \frac{\boldsymbol{T}_i^n}{I}, \quad \boldsymbol{\theta}_i^{n+1} = \boldsymbol{\theta}_i^n + \Delta t \boldsymbol{\omega}_i^n \ . \tag{13}$$

It is difficult to determine theoretically an appropriate time step in Eqs. (12) and (13), because multiscale forces are exerted on spheres and movement velocity of spheres cannot be estimated. Thus, the time step is empirically determined as large as possible in so far as ensuring a stable calculation.

A three-dimensional computational region is divided into a number of unit cubic cells. The index of the cell in which center of each sphere is contained, is obtained at the beginning of every time step. Utilization of the information of cell index for each sphere can remarkably reduce the computational cost to find a pair of spheres between which contact force, electrostatic force and van der Waals force are exerted. To find a pair of spheres between which lateral capillary immersion force is exerted, it is necessary to search for counterpart spheres that are visible from each sphere on the interface. Firstly, neighboring spheres are found by searching cells outward from the cell that contains *i*-th sphere. Secondly, perspective angle of

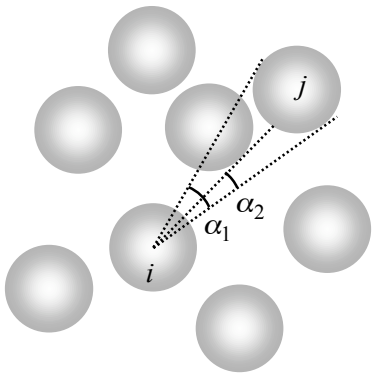

Fig. 3 Calculation of visible ratio $\beta_{ij} = \alpha_2 / \alpha_1$

each neighboring sphere is obtained by drawing tangents from the center of *i*-th sphere. Finally, visible ratio of each neighboring sphere is calculated, as shown in Figure 3. The lateral capillary immersion force is exerted between *i*-th sphere and spheres that have the visible ratio more than zero. Note that the visible ratio is multiplied by the magnitude of the force in Eq. (6).

3 Simulation results

3.1 Computational conditions

Performance of the present simulator is demonstrated by drying simulations of suspension films on a flat substrate. Computational conditions are chosen as follows: A computational region is a cuboid with a square bottom. Width of the region is 1.35 μm and height is 150 nm that is equal to initial thickness of the suspension films. A periodic boundary condition is imposed on four vertical faces of the region. The volume fractions of nanoparticles in the suspension films are 0.2 and 0.4, in which the numbers of nanoparticles are 841 and 1683, respectively. In these cases, the coverage ratio, which is equal to 1 when the computational region is covered with a monolayer of hexagonally close-packed nanoparticles, are 1.0 and 2.0, respectively. The diameter and the zeta potential of the nanoparticles are 50 nm and -50 mV, respectively. The temperature and the viscosity of the solvent are 20 ˚C and 0.001 Ns/m^2, respectively. The contact angle on the nanoparticles is 60˚. The frictional coefficient between the nanoparticles and between the nanoparticles and the substrate are 0.2 and 0.02, respectively. The simulation time is 15 μs and the time step is 0.01ns. The present simulations are carried out on a personal computer of symmetric multi processors (dual Intel Xeon 3.06 GHz) with a Linux operating system and a FORTRAN compiler. The CPU time is 2.0 hours for the coverage ratio of 1.0 and 6.5 hours for the coverage ratio of 2.0.

In the case of computational conditions described above, the magnitude of forces exerted on a partially immersed nanoparticles on the substrate as a function of intersurface distance is illustrated in Figure 4. It is indicated that the active range of each force is so different that the magnitude relation of these forces considerably changes with the intersurface distance. Since the intersurface distance can change from several times the sphere size to zero during drying, one can say that any forces cannot be neglected in the numerical model.

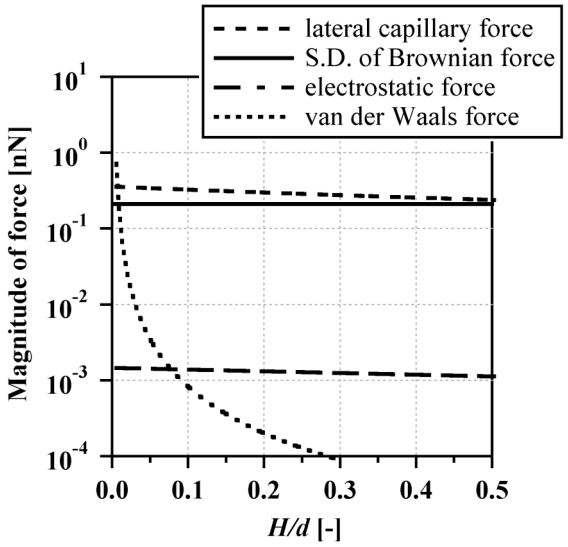

Fig.4 Magnitude of forces exerted on a nanoparticle (h/d = 0.625)

3.2 Structure formation of nanoparticles

Figure 5 shows snapshots of nanoparticles in the suspension films as a function of thickness of the suspension films. At the beginning of simulations, nanoparticles are randomly located in

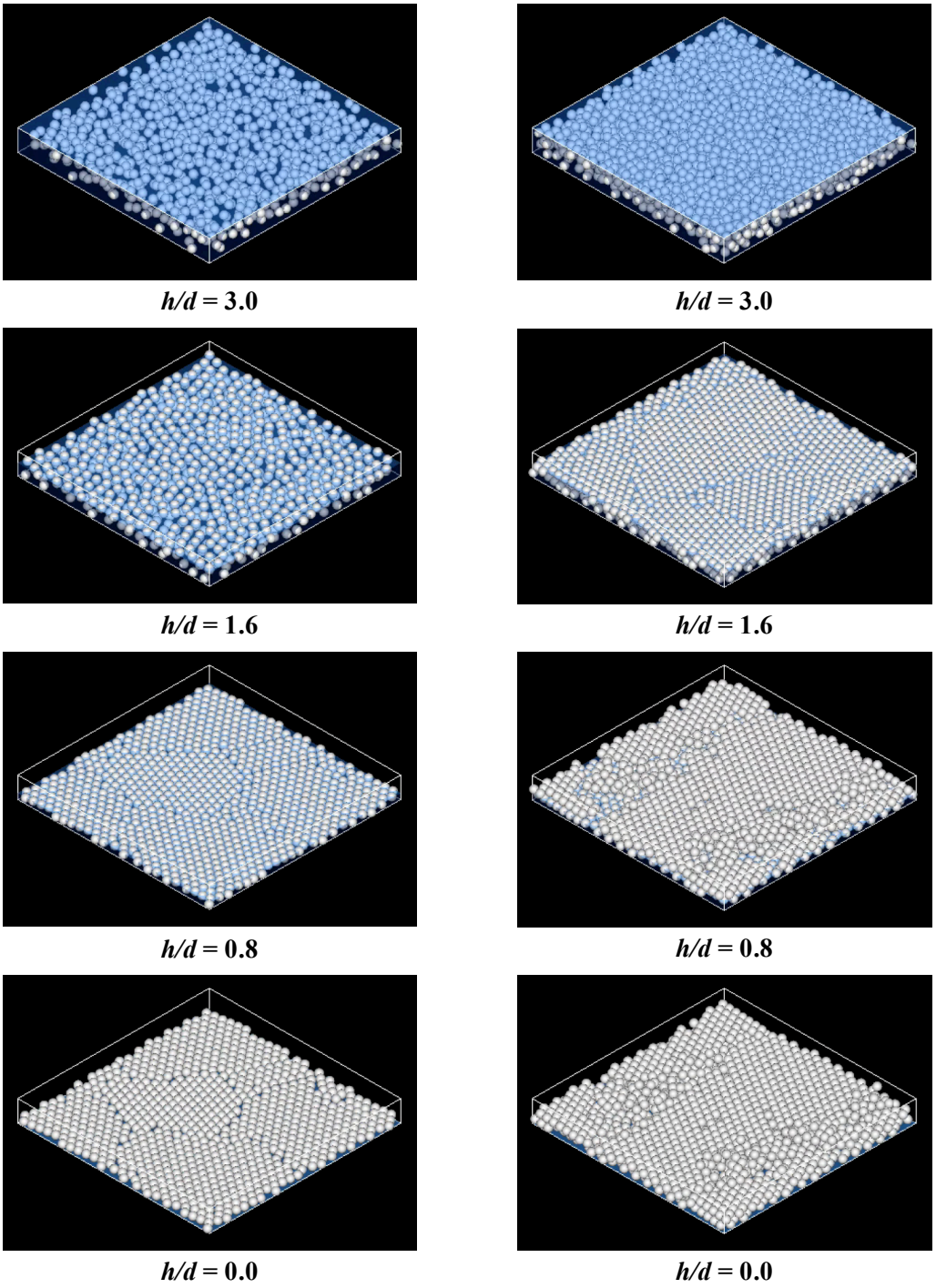

(a) coverage ratio = 1.0 (b) coverage ratio = 2.0

Fig. 5 Snapshots of nanoparticles in suspensions during drying

the suspension films in Figure 5(a) and (b). The nanoparticles move downward along with the interface because vertical capillary force is exerted on nanoparticles that contact with the interface. In the case of the coverage ratio of 1.0, all nanoparticles are deposited on the substrate and planar colloidal crystals are formed at $h/d = 0.8$. As the suspension film gets thinner, lateral capillary force is exerted on all nanoparticles and a planar crystalline structure with some defects is formed at the end of simulation. On the other hand, in the case of the coverage ratio of 2.0, upper-layered nanoparticles in the suspension film form a planar colloidal crystals at $h/d = 1.6$, because downward motion of the nanoparticles that contact with the interface is prevented

by lower-layered nanoparticles that are deposited on the substrate. As the suspension film gets thinner, some nanoparticles are pushed on to the upper layer due to lateral capillary forces exerted among nanoparticles, as shown in the figure at h/d=0.8. Finally, the nanoparticles form a double layer crystalline structure with some defects and some overspills on the upper layer.

In order to explain the structure formation described above quantitatively, isotropic ordering factor (IOF) defined by the authors[8], is employed to quantify the planar structures of nanoparticles. The IOF is the ratio of the number of equilateral polygons to the number of all polygons that are generated by the Voronoi tessellation of a planar distribution of nanoparticle centers. The IOF is 0 if all nanoparticles are randomly distributed, and 1 if all nanoparticles form an isotropic crystalline structure. Figure 6 shows IOF of the planar structures of nanoparticles as a function of thickness of the suspension film. In the case of the coverage ratio of 1.0, IOF rapidly increases at h/d = 0.8, because all nanoparticles are deposited on the substrate at that time. The IOF increases again at h/d = 0.3 in which planar crystallization of nanoparticles occurs by lateral capillary force. On the other hand, in the case of the coverage ratio of 2.0, the lower-layered nanoparticles are deposited on the substrate and the upper-layered nanoparticles are deposited on the lower-layered nanoparticles at h/d = 1.6. At that time, the upper- and lower-layered nanoparticles simultaneously form colloidal crystals. Final value of IOF of the lower layer is larger than that of the upper layer, because the upper layer suffers from some defects caused by the overspills on the upper layer.

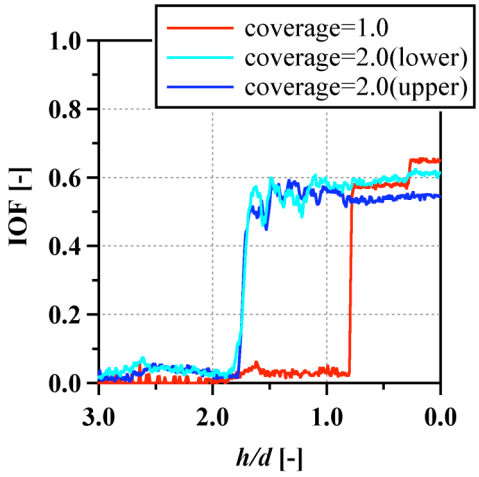

Fig. 6 IOF of planar structures of nanoparticles as a function of thickness of suspension film

4 Conclusions

A three-dimensional structure formation simulator of nanoparticles in a suspension film during drying has been developed. The simulator reproduced structure formations of monolayer and multilayer of nanoparticles on a substrate after drying. The processes of structure formations were visualized, and planar structures of nanoparticles were evaluated temporally and quantitatively using the positions of nanoparticles. The simulation results revealed the moment of structure formation and the primary mechanism of structure formation as follows: Nanoparticles in a suspension film form a layered structure as thickness of the suspension film gets thinner, because nanoparticles are captured on the gas-liquid interface by vertical capillary force. When nanoparticles are deposited on the substrate or on other nanoparticles that are deposited on the substrate, they are subject to lateral capillary immersion force and form a crystalline structure. In the case of structure formation of double-layered nanoparticles, the structure formation of upper-layered nanoparticles causes the structure formation of the lower-layered nanoparticles. Future parametric studies by the present simulator may clarify the relationship between process parameters and three-dimensional structures of nanoparticles.

5 Nomenclatures

A	= Hamaker constant	[Nm]
d	= diameter of nanoparticle	[m]
e	= elementary electric charge	[C]
$\boldsymbol{F}^{\mathrm{ca}}$	= capillary force vector	[N]
$\boldsymbol{F}^{\mathrm{co}}$	= contact force vector	[N]
$\boldsymbol{F}^{\mathrm{e}}$	= electrostatic force vector	[N]
$\boldsymbol{F}^{\mathrm{w}}$	= van der Waals force vector	[N]
$\boldsymbol{F}^{\mathrm{n}}$	= normal contact force vector	[N]
$\boldsymbol{F}^{\mathrm{t}}$	= tangential contact force vector	[N]
f^{e}	= magnitude of electrostatic force	[N]
f^{l}	= magnitude of lateral capillary immersion force	[N]
f^{v}	= magnitude of vertical capillary force	[N]
f^{w}	= magnitude of van der Waals force	[N]
H	= intersurface distance	[m]
h	= thickness of suspension film	[m]
I	= inertial moment of sphere	[kgm^2]
k_{b}	= Boltzmann constant	[Nm/K]
L	= distance between centers of two spheres	[m]
m	= mass of sphere	[kg]
n	= number density of electrolyte ions	[1/m^3]
$\boldsymbol{n}$	= unit normal vector	[-]
$\boldsymbol{R}$	= Brownian force vector	[N]
r	= radius of sphere	[m]
r_{c}	= radius of interface circle on sphere	[m]
$\boldsymbol{s}$	= unit vector normal to interface	[-]
T	= absolute temperature of suspension film	[K]
$\boldsymbol{T}^{\mathrm{co}}$	= contact torque vector	[Nm]
t	= time	[s]
$\boldsymbol{V}$	= velocity vector of sphere	[m/s]
$\boldsymbol{X}$	= position vector of sphere	[m]
Z	= electrolyte ionic valency	[-]
α	= perspective angle	[rad]
β	= visible ratio	[-]
Δt	= time step	[s]
ε_0	= permittivity of vacuum	[C^2/Nm^2]
ε_{r}	= relative permittivity of solvent	[-]
φ	= zeta potential	[V]
γ	= surface tension	[N/m]
μ	= friction coefficient	[-]
$\boldsymbol{\theta}$	= rotation angle vector of sphere	[rad]
σ	= standard deviation of Brownian random force	[N]
$\boldsymbol{\omega}$	= angular velocity vector of sphere	[rad/s]
ξ	= coefficient of Stokes drag for sphere	[kg/s]
ψ	= slope angle of interface on sphere	[rad]

6 References

1. Denkov, N. D., Velev, O. D., Kralchevsky, P. A., Ivanov, I. B., Yoshimura, H. and Nagayama, K., 1992, Mechanism of Formation of Two-Dimensional Crystals from Latex Particles on Substrates, *Langmuir*, **8**, 3183-3190
2. Rodner, S. C., Wedin, P. and Bergstrom, L., 2002, Effect of Electrolyte and Evaporation Rate on the Structural Features of Dried Silica Monolayer Films, *Langmuir*, **18**, 9327-9333
3. Okubo, T., Chujo, S., Maenosono, S. and Yamaguchi, Y., 2003, Microstructure of silica particle monolayer films formed by capillary immersion force, *J. Nanopart. Res.*, **5**, 111-117
4. Motte, L., Lacaze, E., Maillard, M. and Pileni, M. P., 2000, Self-Assemblies of Silver Sulfide Nanocrystals on Various Substrates, *Langmuir*, **16**, 3803-3812
5. Kralchevsky, P. A. and Nagayama, K., 2001, Particles at Fluid Interfaces and Membranes – Attachment of Colloid Particles and Proteins to Interfaces and Formation of Two-Dimensional Arrays, Elsevier, Amsterdam, Netherlands
6. Maenosono, S., Dushkin, C. D., Yamaguchi, Y., Nagayama, K. and Tsuji, Y., 1999, Effect of Growth Conditions on the Structure of Two-dimensional latex crystals: modeling, *Col. Polym. Sci.*, **277**, 1152-1161
7. Nishikawa, H., Maenosono, S., Yamaguchi, Y. and Okubo, T., 2003, Self-assembling process of colloidal particles into two-dimensional arrays induced by capillary immersion force: A simulation study with discrete element method, *J. Nanopart. Res.*, **5**, 103-110
8. Fujita, M., Nishikawa, H., Okubo, T. and Yamaguchi, Y., 2004, Multiscale Simulation of Two-Dimensional Self-Organization of Nanoparticles in Liquid Film, *Jpn. J. Appl. Phys.*, **43**, 4434-4442
9. Nishikawa, H., Morozumi, K., Hu, M., Okubo, T., Fujita, M., Yamaguchi, Y. and Okubo, T., 2005, Effects of Particle Size on the Monolayer Structure of Nanospheres Formed via a Coating-Drying Process, *J. Chem. Eng. Jpn.* (in press)
10. Cundall, P. A. and Strack, O. D. L., 1979, A discrete numerical model for granular assemblies, Geotechnique, **29**, 47-65
11. Tsuji, Y., Tanaka, T. and Ishida, T., 1992, Lagrangian numerical simulation of plug flow of cohesionless particles in a horizontal pipe, Powder Tech., **71**, 239-250
12. Fujita, M. and Yamaguchi, Y., Development of Three-Dimensional Structure Formation Simulator of Colloidal Nanoparticles during Drying, *J. Chem. Eng. Jpn.*, (submitted)
13. Israelachvili, J. N., 1992, Intermolecular and Surface Forces, Academic Press, London, U.K.
14. Ermak, D. L. and McCammon, J. A., 1978, Brownian dynamics with hydrodynamic interactions, J. Chem. Phys. **69**, 1352-1360.